Check for updates

Improved Epitaxy of AlN Film for Deep-Ultraviolet Light-Emitting Diodes Enabled by Graphene

Zhaolong Chen, Zhiqiang Liu, Tongbo Wei, Shenyuan Yang, Zhipeng Dou, Yunyu Wang, Haina Ci, Hongliang Chang, Yue Qi, Jianchang Yan, Junxi Wang, Yanfeng Zhang, Peng Gao,* Jinmin Li,* and Zhongfan Liu**

The growth of single-crystal III-nitride films with a low stress and dislocation density is crucial for the semiconductor industry. In particular, AlN-derived deep-ultraviolet light-emitting diodes (DUV-LEDs) have important applications in microelectronic technologies and environmental sciences but are still limited by large lattice and thermal mismatches between the epilayer and substrate. Here, the quasi-van der Waals epitaxial (QvdWE) growth of high-quality AlN films on graphene/sapphire substrates is reported and their application in high-performance DUV-LEDs is demonstrated. Guided by density functional theory calculations, it is found that pyrrolic nitrogen in graphene introduced by a plasma treatment greatly facilitates the AlN nucleation and enables fast growth of a mirror-smooth single-crystal film in a very short time of ≈0.5 h (≈50% decrease compared with the conventional process), thus leading to a largely reduced cost. Additionally, graphene effectively releases the biaxial stress (0.11 GPa) and reduces the dislocation density in the epilayer. The as-fabricated DUV-LED shows a low turn-on voltage, good reliability, and high output power. This study may provide a revolutionary technology for the epitaxial growth of AlN films and provide opportunities for scalable applications of graphene films.

Group-III nitrides (III-Ns) are widely used for light-emitting diodes (LEDs), lasers, and high-power/high-frequency electronic devices due to their direct wide band gap and stability.[1–4] Current state-of-the-art commercial III-N films are usually heteroepitaxially grown on *c*-sapphire,[1] 6H-SiC,[1] and Si (111),[5] by metal–organic chemical vapor deposition (MOCVD). However, large lattice and thermal mismatches between these substrates and epilayers lead to a high defect density and large biaxial stress[6–8] and also greatly degrade the performance of the III-N devices. Usually, a time-consuming low-temperature buffer (LT) layer is required to diminish the impact of the mismatch.[9] However, the high migration barrier of atoms on the substrate and high bond energy of the III-N always lead to a three-dimensional (3D) island growth mode, especially for AlN on a sapphire substrate, which requires a very

Z. L. Chen, Prof. Z. Q. Liu, Prof. T. B. Wei, Y. Y. Wang, H. L. Chang, Dr. J. C. Yan, Prof. J. X. Wang, Prof. J. M. Li
State Key Laboratory of Solid-State Lighting
Institute of Semiconductors
Chinese Academy of Sciences
Beijing 100083, China
E-mail: tbwei@semi.ac.cn; jmli@semi.ac.cn

Z. L. Chen, H. N. Ci, Y. Qi, Prof. Y. F. Zhang, Prof. P. Gao, Prof. Z. F. Liu
Center for Nanochemistry (CNC)
Beijing Science and Engineering Center for Nanocarbons
College of Chemistry and Molecular Engineering
Peking University
Beijing 100871, China
E-mail: p-gao@pku.edu.cn; zfliu@pku.edu.cn

Z. L. Chen, H. N. Ci, Y. Qi, Prof. Z. F. Liu
Beijing National Laboratory for Molecular Sciences
Beijing 100871, China

Prof. S. Y. Yang, Prof. Z. Q. Liu, Prof. T. B. Wei, Dr. J. C. Yan, Prof. J. X. Wang, Prof. J. M. Li
Center of Materials Science and Optoelectronics Engineering
University of Chinese Academy of Science
Beijing 100049, China

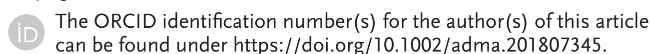
The ORCID identification number(s) for the author(s) of this article can be found under https://doi.org/10.1002/adma.201807345.

Prof. S. Y. Yang
School of Microelectronics
University of Chinese Academy of Sciences
Beijing 101408, China

Prof. S. Y. Yang
State Key Laboratory of Superlattices and Microstructures
Institute of Semiconductors
Chinese Academy of Sciences
Beijing 100083, China

Z. P. Dou, Prof. P. Gao
Electron Microscopy Laboratory, and International Center for Quantum Materials
School of Physics
Peking University
Beijing 100871, China

Prof. P. Gao
Collaborative Innovation Centre of Quantum Matter
Beijing 100871, China

Prof. Z. F. Liu
Beijing Graphene Institute (BGI)
Beijing 100095, P. R. China

DOI: 10.1002/adma.201807345

 © 2019 WILEY-VCH Verlag GmbH & Co. KGaA, Weinheim

thick coalescence thickness that increases the MOCVD growth time and cost.

Recently, single-crystal materials have been epitaxially grown on 2D material-coated substrates due to remote atomic interactions between the substrate and epilayers.[6,10] In particular, graphene is a thermally stable material with an atomically flat surface and excellent mechanical, electrical, and thermal properties, making it an ideal buffer layer. The van der Waals epitaxial (vdWE) growth of III-N films on a graphene/substrate system has also been proposed to effectively reduce the mismatch effect due to the weak bonds between III-N and graphene and further alleviate the self-heating issue or achieve transferable optoelectronics and electronics.[10–14] Moreover, the low diffusion barrier of adatoms on graphene potentially enables fast growth of III-N films with a reduced coalescence thickness. However, the main challenge is that the dangling-bond-free feature of graphene suppresses III-N nucleation,[12] limiting the growth of large-area single crystals. Although there are a few reported works on the growth of GaN on graphene targeted to mature blue LEDs,[2,11–13] growth of AlN films that enable deep-ultraviolet LEDs (DUV-LEDs) for applications in air purification, water purification, and germicidal and biomedical instrumentation systems[2,15] remains relatively unexplored.

Here, we successfully grow a high-quality AlN film on graphene and fabricate high-performance DUV-LEDs. Guided by density functional theory (DFT) calculations, a N_2 plasma treatment of the graphene that is directly grown on a sapphire substrate is developed to facilitate the AlN nucleation by introducing pyrrolic nitrogen doping. With the presence of an atomically thin graphene film, the substrate still has a weak interaction with the epilayers,[6] insuring fast epitaxial lateral overgrowth of a large-area single-crystal AlN film on graphene with a low stress (0.11 GPa), and low dislocation density even without an LT buffer layer. Therefore, the as-fabricated DUV-LED devices show a low turn-on voltage, good reliability, and high output power. This process can substantially shorten the MOCVD growth time and reduce the cost, which is beneficial to the III-N semiconductor industry.

To avoid the size and repetition limitations associated with transferring graphene from metal substrates onto target substrates, we directly grow the graphene film on *c*-plane (0001) sapphire via a catalyst-free atmosphere chemical vapor deposition (CVD) method.[16] **Figure 1**a shows a photograph of the as-grown 2 inch graphene/sapphire wafer. The as-grown graphene film fully covers the sapphire substrate and shows a high optical transparency of ≈96.7% at 550 nm (Figure S1, Supporting Information) and good uniformity after being transferred onto SiO_2/Si substrates (Figure 1b). The typical Raman spectrum (the black line in Figure 1e) as well as Raman mapping (Figure S2, Supporting Information) exhibit characteristic peaks of graphene at 1348 cm^{-1} (D-band), 1586 cm^{-1} (G-band), and 2680 cm^{-1} (2D-band) with a high microscale uniformity. The monolayer structure and high quality of the film are further confirmed by the transmission electron microscopy (TEM) characterization in Figure 1c,d. X-ray photoelectron spectroscopy (XPS) spectra also verify the high quality of the graphene (Figure S3, Supporting Information). To enhance the reactivity for the subsequent AlN growth, the graphene is treated in N_2-plasma, after which the defect density (n_D) in graphene is increased from $n_D = 2.13 \times 10^{11}$ cm^{-2} to $n_D = 3.23 \times 10^{11}$ cm^{-2} based on the I_D/I_G ratio[17] in Figure 1e, where I is the peak intensity. The nitrogen incorporation is verified by the new N–sp^3C peak (≈286.5 eV) from the XPS spectrum in Figure 1f.[18] The doped nitrogen is identified as pyrrolic N with a content of 5.6% (Figure 1g), while there is no broad peak for the pristine graphene (Figure S4, Supporting Information).

DFT calculations are performed to verify the effects of the introduced pyrrolic N on the AlN nucleation. The adsorption energies of the Al and N adatoms on the hollow, bridge and top sites of the pristine graphene indicate that an Al adatom bonds to graphene more strongly than an N adatom with an adsorption energy of ≈1.1 eV (Figure S5 and Table S1, Supporting Information). The adsorption energy of Al atoms to pyrrolic N in plasma-treated graphene is greatly increased to 5.9–8.6 eV, which shows a substantially enhanced reactivity of graphene to AlN nucleation (Figure 1h). The adsorption of an Al atom partially recovers the honeycomb structure near the N defect but introduces significant structural distortion, and the adjacent C atoms have sp^3-like characteristics. The interfacial binding features of the AlN/Gr are further analyzed by DFT total energy calculations. As shown in Figure 1i, the obvious electron accumulation around the pyrrolic N atom indicates the formation of Al—N bonds. Remarkably, the formation energy (defined as the total energy difference of AlN and plasma-treated graphene before and after bonding) is reduced by more than 0.28 eV$Å^{-2}$ compared with pristine graphene. The pyrrolic N in the plasma-treated graphene tends to have a graphitic N configuration at a high temperature (1200 °C) during the growth of AlN,[19] and it also shows a reduced formation energy of ≈0.004 eV$Å^{-2}$ (Figure S6, Supporting Information). We also find that the occupied $2p_z$ orbital (π-orbital) intensity of the C atom near the N atom is obviously decreased, as shown in the projected density of states (PDOS) of the $2p_z$ orbitals on different C atoms (Figure 1j). This suggests a transformation of sp^2- to sp^3-like hybridization for the C atoms near an N defect and electronic coupling between the C π and N π orbitals. Therefore, an N_2 plasma treatment greatly facilitates AlN nucleation by the formation of Al—N bonds.

As schematically shown in **Figure 2**a, AlN nucleation should primarily occur at N-defect sites through Al—N bonds, and then 2D lateral growth of the AlN islands is greatly promoted to form a continuous film due to the reduced diffusion barrier of adatoms on the ideal graphene.[20] To experimentally verify the superiority of plasma-treated graphene films for AlN growth, we grow AlN nuclei and films on bare sapphire and plasma-treated graphene/sapphire substrates under the same conditions for comparison. This shows that the nucleation density on N_2-plasma-treated graphene is increased more than ten times compared with that on bare sapphire, and the uniformity is also greatly improved (Figure 2b,c). In contrast, on the bare sapphire substrate, the hexagonal AlN grains are large and widely distributed in size (Figure 2c and Figure S7a, Supporting Information). During the subsequent coalescence process, the AlN on sapphire forms 3D AlN clusters with grain sizes of several hundred nanometers (Figure S7b, Supporting Information), while on plasma-treated graphene, the AlN film is continuous and smooth (Figure 2d and inset) with an atomically terraced surface and root-mean-square (RMS) roughness of ≈0.27 nm, as shown in Figure 2e. This process is even much

© 2019 WILEY-VCH Verlag GmbH & Co. KGaA, Weinheim

15214095, 2019, 23, Downloaded from https://onlinelibrary.wiley.com/doi/10.1002/adma.201807345 by Zhejiang University, Wiley Online Library on [04/09/2023]. See the Terms and Conditions (https://onlinelibrary.wiley.com/terms-and-conditions) on Wiley Online Library for rules of use; OA articles are governed by the applicable Creative Commons License

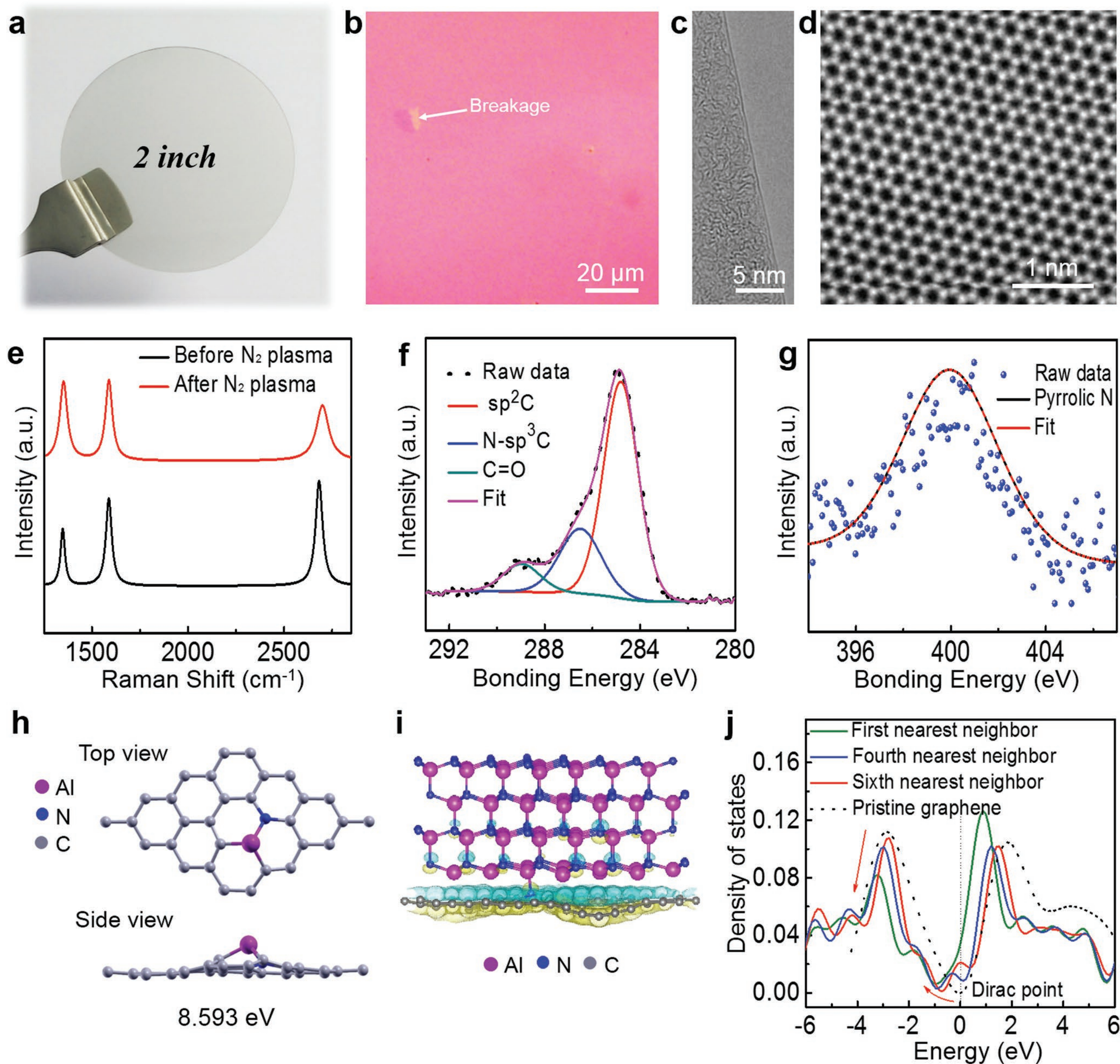

Figure 1. Direct growth of graphene on sapphire substrate and its surface modification by N_2 plasma treatment. a) Photograph of an as-grown 2 inch graphene/sapphire wafer. b) Optical microscopy (OM) image of the transferred graphene film on SiO_2/Si. c) High-resolution transmission electron microscopy (HRTEM) image on the edge of the graphene film showing its monolayer structure. d) Representative atomically resolved Z-contrast image of graphene revealing its good quality. e) Raman spectra of graphene film before N_2 plasma treatment (black) and after N_2 plasma treatment (red). f) C 1s X-ray photoelectron spectroscopy (XPS) spectrum of N_2-plasma-treated graphene film, showing the characteristic signals of graphene with an sp^2 carbon peak (≈284.8 eV), an N–sp^3 peak (≈286.5 eV), and a broad O—C=O peak (≈288.9 eV). g) N 1s XPS spectrum of N_2-plasma-treated graphene film, showing the characteristic signals of a pyrrolic N feature (≈400.1 eV). h) Density functional theory (DFT) calculations of the bonding of one Al adatom on pyrrolic N with a bonding energy of 8.593 eV. i) Atomic model structures and isosurfaces of electron density difference of AlN on N_2-plasma-treated graphene via Al—N bond. The blue and yellow isosurfaces correspond to charge depletion and accumulation, respectively, with isosurface values of $\pm$ 0.0001 e Å^{-3}. j) Calculated projected density of states (PDOS) of $2p_z$ orbitals (π-orbital) of three C atoms with different distances to the N atom: the first nearest neighbor, the second nearest neighbor, and the sixth nearest neighbor.

faster than that with the LT buffer layer (Figure S8, Supporting Information). The *c*-axis-oriented hexagonal wurtzite in the single-crystal AlN is confirmed by a large-scale view of electron backscatter diffraction (EBSD) maps (Figure S9, Supporting Information) and high-resolution X-ray diffraction (XRD) spectra (Figure S10, Supporting Information). We also grow AlN on pristine graphene/sapphire under the same conditions for comparison and find that the quality of the AlN film on plasma-treated graphene/sapphire is much better (see details in Figure S11, Supporting Information).

© 2019 WILEY-VCH Verlag GmbH & Co. KGaA, Weinheim

15214095, 2019, 23, Downloaded from https://onlinelibrary.wiley.com/doi/10.1002/adma.201807345 by Zhejiang University, Wiley Online Library on [04/09/2023]. See the Terms and Conditions (https://onlinelibrary.wiley.com/terms-and-conditions) on Wiley Online Library for rules of use; OA articles are governed by the applicable Creative Commons License

15214095, 2019, 23, Downloaded from https://onlinelibrary.wiley.com/doi/10.1002/adma.201807345 by Zhejiang University, Wiley Online Library on [04/09/2023]. See the Terms and Conditions (https://onlinelibrary.wiley.com/terms-and-conditions) on Wiley Online Library for rules of use; OA articles are governed by the applicable Creative Commons License

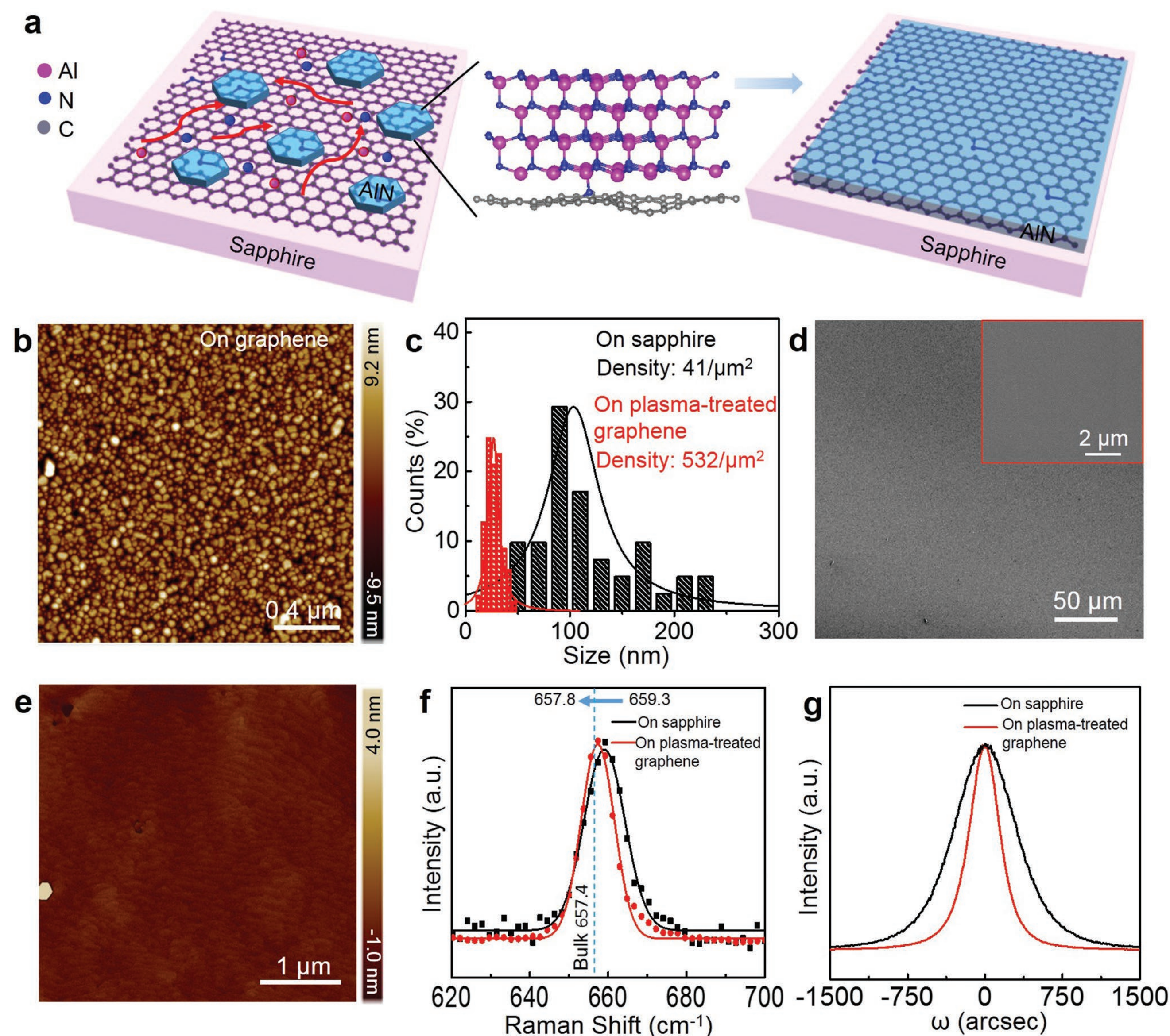

Figure 2. Fast AlN nucleation and film growth on N_2-plasma-treated graphene/sapphire substrate. a) Schematic diagram of the nucleation and film growth of AlN on N_2-plasma-treated graphene/sapphire substrate. 1) Enhanced AlN nucleation on plasma-treated graphene/sapphire substrate through Al—N bonding. 2) Then, the fast 2D lateral growth of the AlN islands to form a continuous film due to the reduced diffusion barrier of adatoms on the ideal graphene. b) Atomic force microscopy (AFM) height image of AlN nucleation on plasma-treated graphene/sapphire substrate (1200 °C, 500 sccm N_2, 50 sccm H_2, 15 sccm TMAl, 6 min). c) Density and size distribution analysis of AlN nucleation on sapphire and plasma-treated graphene/sapphire substrate. d) Scanning electron microscopy (SEM) image of as-grown AlN film on plasma-treated graphene/sapphire substrate with increasing growth time to 1 h. e) AFM height image of as-grown AlN film on plasma-treated graphene/sapphire substrate, showing atomically flat feature with RMS roughness ≈0.27 nm. f) Raman spectra of AlN films grown on sapphire (black line) and plasma-treated graphene (red line). g) X-ray rocking curves of (0002) AlN grown on sapphire (black line) and plasma-treated graphene (red line).

The QvdWE growth of AlN on plasma-treated graphene is also expected to release the biaxial stress and reduce the dislocation density in the epilayer. The Raman spectrum of the E_2 phonon mode of AlN that is sensitive to the stress is used to evaluate the biaxial stress.[21,22] With the N_2 plasma-treated graphene layer, the E_2 peak of the AlN is located at 657.8 cm^{-1}, almost identical to the stress-free AlN (657.4 cm^{-1}) in Figure 2f.[23] For comparison, we also grow AlN film on sapphire with a conventional LT buffer layer, which shows a larger frequency (569.2 cm^{-1}) due to the high compressive strain. Based on these measurements, we estimate that the residual stress of AlN is significantly reduced from 0.49 to 0.11 GPa by the plasma-treated graphene.[24] In fact, the huge stress in the AlN film on bare sapphire usually causes cracks at the edge of the wafer, while none are observed in the plasma-treated graphene buffered sample (Figure S12, Supporting Information). The (0002) full width at half maximum (FWHM) of the X-ray ω-scan (rocking curve) of the AlN epilayer is significantly reduced

 © 2019 WILEY-VCH Verlag GmbH & Co. KGaA, Weinheim

15214095, 2019, 23, Downloaded from https://onlinelibrary.wiley.com/doi/10.1002/adma.201807345 by Zhejiang University, Wiley Online Library on [04/09/2023]. See the Terms and Conditions (https://onlinelibrary.wiley.com/terms-and-conditions) on Wiley Online Library for rules of use; OA articles are governed by the applicable Creative Commons License

from 698.6 to 315.5 arcsec with the assistance of graphene in Figure 2g, and its $(10\bar{1}2)$ FWHM is also reduced from 884.2 to 518 arcsec (Figure S13, Supporting Information). The estimated densities of the screw and edge dislocations in the as-grown AlN without graphene are 1.06×10^9 and 6.29×10^9 cm^{-2}, respectively, while they are reduced to 2.67×10^8 and 2.45×10^9 cm^{-2} on the plasma-treated graphene.[25] Therefore, the stress of the epilayer is largely released, and the dislocation density of the as-grown AlN on plasma-treated graphene is comparable with that typically obtained via conventional LT buffer-assisted epitaxy on sapphire substrates.[26]

The epitaxial relationship between the epilayer and *c*-plane sapphire substrate through the graphene is explored by performing grazing incidence XRD and cross-sectional scanning transmission electron microscopy (STEM). The XRD ϕ scan (**Figure 3**a) and selected area electron diffraction (SAED) patterns (Figure 3b) reveal that the AlN unit cells are rotated by 30° with respect to the sapphire and through the graphene, as schematically shown in Figure 3c, which is in good agreement with previous reports of epitaxial wurtzite III-Ns on sapphire.[27,28] In addition, the energy-dispersive X-ray spectroscopy (EDX) mapping analysis of Al Kα shows a sub-nanometer gap between the AlN and Al_2O_3 (Figure 3e), in sharp contrast to that on the bare Al_2O_3 sample (Figure S14, Supporting Information), confirming the existence of a graphene interlayer after AlN growth. The atomically resolved STEM image shows a sharp interface of Al_2O_3/graphene/AlN (Figure 3d,f), where the graphene exhibits faint contrast between the epitaxial layer and the substrate in the Z-contrast image.

We also adjusted the graphene film thickness from ≈1 layer to ≈5 layers to verify the effect of the graphene layer number on the quality of the epitaxial AlN films. The thickness of the graphene film can be controlled by the growth time, as confirmed by optical transmittance (Figure S15, Supporting Information). The ω-scan XRD is performed to estimate the quality of as-grown AlN films with different thicknesses of the graphene buffer layer (Figure S16, Supporting Information). The (0002) FWHM of the AlN is smallest when the thickness of graphene is ≈1–2 layers.

Thus, a high-quality AlN film on a plasma-treated graphene/sapphire substrate enables DUV-LED fabrication. The schematic structure of an AlGaN DUV-LED is shown in **Figure 4**a, consisting of a p-GaN hole injection layer, a 50 nm thick layer of Mg-doped p-AlGaN, five-period $Al_{0.4}Ga_{0.6}N/Al_{0.5}Ga_{0.5}N$ multiquantum wells

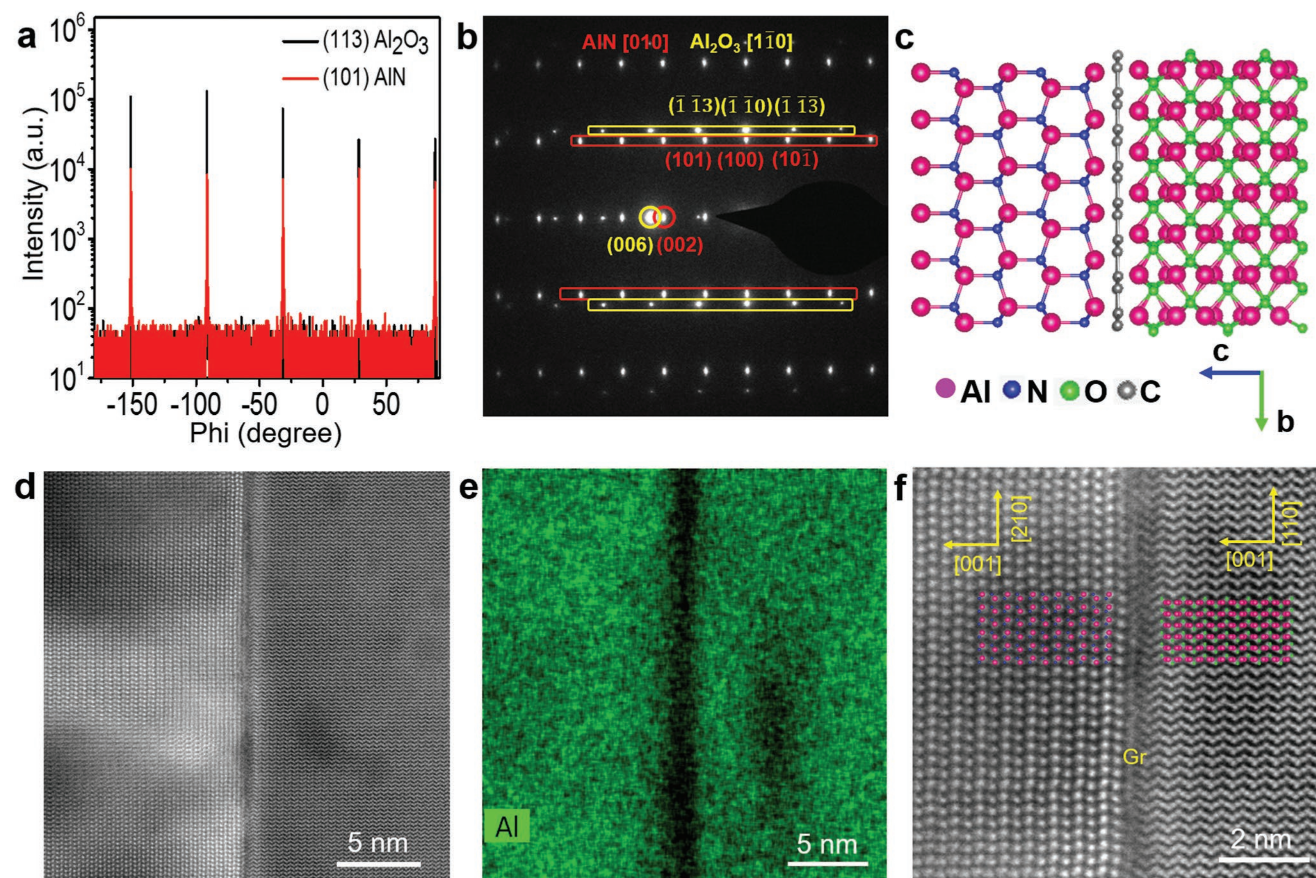

Figure 3. Interfacial bonding and epitaxial relationship between epilayer and *c*-plane sapphire substrate with plasma-treated graphene. a) Grazing-incidence X-ray diffraction azimuthal off-axis phi scan for Al_2O_3 (113) and AlN (101). b) Selected-area electron diffraction pattern taken at an AlN/graphene/sapphire interface. c) Schematic illustration of the epitaxial relationship between the epilayer and *c*-plane sapphire substrate through graphene. d) High-magnification cross-sectional scanning transmission electron microscopy (STEM) image of the AlN/graphene/Al_2O_3 interface. e) Corresponding energy dispersive X-ray spectroscopy mapping of Al element showing the graphene gap between AlN and Al_2O_3. f) Atomically resolved STEM image of the interface of Al/graphene/Al_2O_3, showing a 30° rotation between AlN and Al_2O_3.

 © 2019 WILEY-VCH Verlag GmbH & Co. KGaA, Weinheim

15214095, 2019, 23, Downloaded from https://onlinelibrary.wiley.com/doi/10.1002/adma.201807345 by Zhejiang University, Wiley Online Library on [04/09/2023]. See the Terms and Conditions (https://onlinelibrary.wiley.com/terms-and-conditions) on Wiley Online Library for rules of use; OA articles are governed by the applicable Creative Commons License

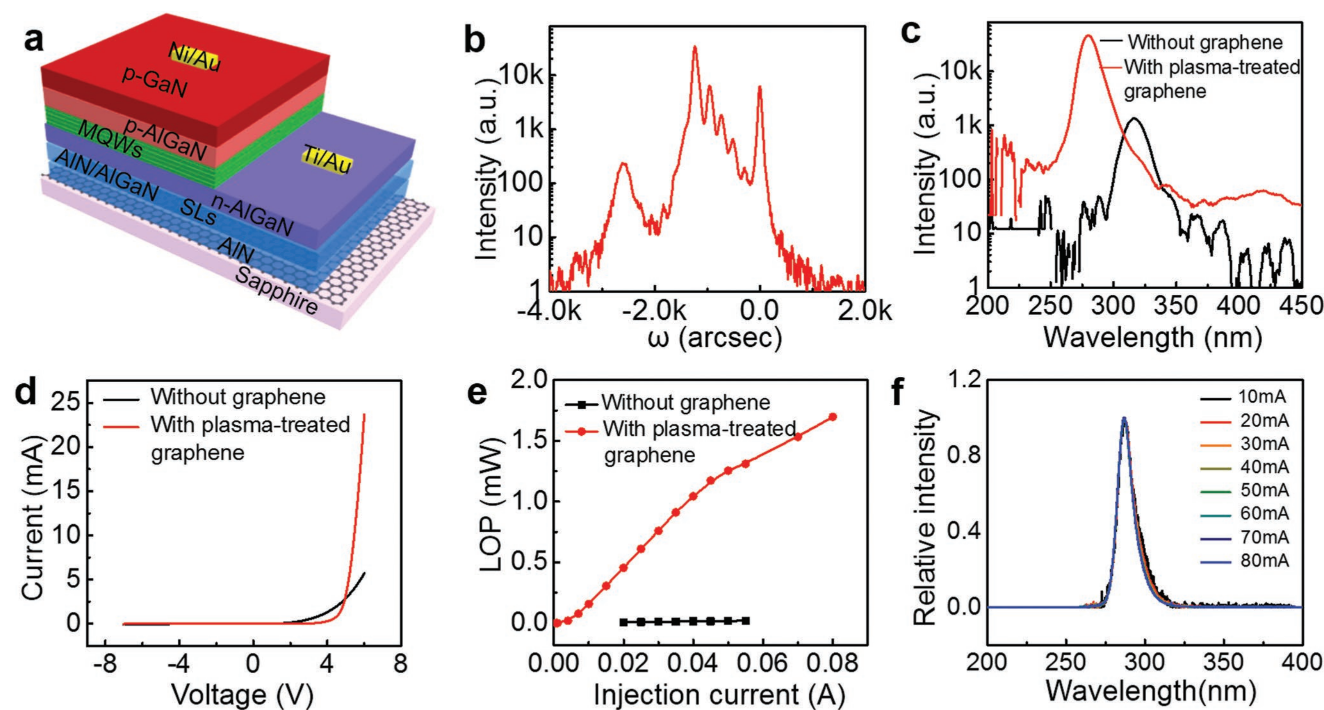

Figure 4. The structure and electroluminescence of as-fabricated DUV-LEDs. a) Schematic illustration of the DUV-LED structure. b) X-ray ω–2θ scan of DUV-LED grown on plasma-treated graphene/sapphire. c) Electroluminescence (EL) spectra of the DUV-LEDs with and without graphene interlayer. d) Current–voltage curves of the as-fabricated DUV-LEDs with and without graphene interlayer. e) Light output power of the as-fabricated DUV-LED with and without graphene interlayer as a function of injection current. f) The normalized EL spectra of DUV-LEDs on graphene/sapphire with currents ranging from 10 to 80 mA.

(MQWs), 2 µm thick Si-doped n-$Al_{0.55}Ga_{0.45}N$, 20-period AlN/AlGaN superlattices, and 1 µm AlN on a plasma-treated graphene/sapphire substrate. The SEM image shows that the surface of the as-grown DUV-LED structure on the plasma-treated graphene/sapphire substrate is continuous and smooth with an RMS roughness of ≈1.56 nm (Figure S17a,b, Supporting Information). The X-ray ω–2θ scan profile shows intense satellite peaks of the AlN/AlGaN superlattice heterostructure on graphene/sapphire substrates, guaranteeing the subsequent high quality of the MQW heterostructure (Figure 4b). For comparison, on bare sapphire, the surface of the LED is irregular with many holes and ravines, and the corresponding RMS roughness is ≈31.7 nm (Figure S17c,d, Supporting Information). The satellite peaks of the superlattice are too weak to be observed (Figure S18, Supporting Information).

The electroluminescence (EL) characteristics of the DUV-LEDs with and without plasma-treated graphene are further evaluated. A typical EL spectrum from the DUV-LED with graphene shows strong luminescence at the peak wavelength of 280 nm. In comparison, the intensity of the DUV-LED without graphene is nearly two orders of magnitude weaker than that with graphene (peak wavelength ≈316 nm, Figure 4c), which originates from the high density of defects. Moreover, the current–voltage curve of the DUV-LED with graphene shows good rectifying behavior with a turn-on voltage of 4.6 V (Figure 4d, red line), and the leakage current measured at −4 V is ≈3 mA. These results are comparable with previous reports.[29,30] On the other hand, the current–voltage curve of the LED without graphene shows a much lower current under the same input voltage and a much higher turn-on voltage (Figure 4d, black line). The light output power (LOP) of the LEDs on graphene/sapphire is linear with an input voltage and a slope efficiency of ≈20 µW mA^{-1}, suggesting that the EL emission is generated from the carrier injection and radiative recombination at the MQW layers (Figure 4e, red line). The external quantum efficiency of the fabricated DUV-LED with graphene is ≈0.5%. In addition, the DUV-LED with graphene shows no shift in peak positions under different currents, indicating a substantial stress relaxation due to the QvdWE growth (Figure 4f). These results indicate that high-performance DUV-LEDs can be directly grown on plasma-treated graphene/sapphire substrates without LT buffer layers, which would greatly shorten the MOCVD growth time and thus reduce the cost (Figure S19, Supporting Information). Therefore, the present work proposes a promising method for the practical application of graphene in high-power LEDs.

In summary, we have successfully demonstrated QvdWE growth of AlN on sapphire substrates using a graphene interlayer for high-performance DUV-LEDs, which may enable several disruptive technologies. Guided by the DFT calculations, N_2 plasma treatment for graphene prior to nitride growth can greatly facilitate AlN nucleation and increase the growth rate by introducing pyrrolic nitrogen into the graphene. The graphene layer effectively releases the biaxial stress and reduces the dislocation density in the epilayer due to the weak vdW interaction of the AlN/graphene stack, while the epitaxial orientation between the AlN and the substrate remains. Notably, because no LT buffer layer is needed, such a growth process can greatly shorten the MOCVD growth time and thus reduce the cost. The fabricated DUV-LED shows a low turn-on

 © 2019 WILEY-VCH Verlag GmbH & Co. KGaA, Weinheim

voltage, high output power and excellent reliability. This work may enable several revolutionary technologies for epitaxial growth of AlN film and DUV-LEDs and provide opportunities for applications of graphene films.

Experimental Section

CVD Growth of Graphene on Sapphire: Typically, the commercial 2 inch *c*-sapphire substrate was loaded into a three-zone high-temperature furnace. Then, graphene growth was performed at 1055 °C with 500 sccm Ar, 300 sccm H_2, and 30 sccm CH_4 for ≈3–5 h.

MOCVD Growth of AlN on Graphene/Sapphire: The graphene/sapphire substrate was exposed to N_2 plasma treatment (PVA TePla AG, 300 Standard) under 200 Pa with a gas flow of 300 sccm and a power of 50 W for 30 S before being loaded into an MOCVD chamber that was constructed in the laboratory. The high-temperature AlN was grown at 1200 °C for 1 h with an NH_3 flow of 500 sccm and a trimethylaluminum (TMAl) flow of 50 sccm. It was a one-step process that does not use a low-temperature buffer layer.

MOCVD Growth of DUV-LED Structure on Graphene/Sapphire Substrate: The AlGaN-based DUV-LED structure was grown on the AlN/Gr/sapphire template, including 20-period $AlN/Al_{0.7}Ga_{0.3}N$ superlattices (SLs), a 2 µm n-$Al_{0.55}Ga_{0.45}N$ layer, five-period $Al_{0.5}Ga_{0.5}N/Al_{0.4}Ga_{0.6}N$ multiple quantum wells (MQWs), and p-type layers (a 30 nm p-$Al_{0.65}Ga_{0.35}N$ electron-blocking layer, a 50 nm p-AlGaN cladding layer, and a 100 nm p-GaN contact layer). Trimethylgallium (TMGa) was used as a Ga precursor. Silane (SiH_4) and bis(cyclopentadienyl) magnesium (Cp_2Mg) was used for n-type and p-type doping, respectively. A 20-period $AlN/Al_{0.7}Ga_{0.3}N$ superlattice (SL) was grown at a temperature of 1130 °C, with the periodic change of TMAl flow to adjust the deposition component while the TMGa flow of 32 sccm and the NH_3 flow of 500 sccm were kept constant. The thickness of the $AlN/Al_{0.7}Ga_{0.3}N$ layer was 15 nm/15 nm, and the total thickness was 600 nm for 20 periods. Then, the temperature was reduced to 1002 °C, and a silicane flow of 2.34 sccm was introduced for the growth of the 2 µm n-$Al_{0.55}Ga_{0.45}N$ layer. The five-period $Al_{0.5}Ga_{0.5}N/Al_{0.4}Ga_{0.6}N$ MQWs was further grown with a 2.4 nm quantum well and a 12.2 nm quantum barrier by switching the TMAl from 24 sccm to 14 sccm and TMGa from 8 sccm to 7 sccm for each period. A 30 nm thick layer of an Mg-doped p-$Al_{0.65}Ga_{0.35}N$ electron blocking layer, a p-AlGaN cladding layer, and a p-GaN contact layer were subsequently deposited. The SiH_4 was 20 sccm, while the NH_3 was 2500 sccm during the whole growth process. After growth, the p-type layers were annealed in the reactor at 800 °C in N_2 atmosphere for 20 min to activate the Mg acceptors.

DUV-LED Device Fabrication: DUV-LED devices with a die size of 0.5 mm × 0.5 mm were fabricated with the standard LED processes of photolithography, ICP etching, and e-beam evaporation. A Ti/Al/Ti/Au metal stack was deposited on the exposed n-AlGaN as the n-type contact, and an Ni/Au stack was used as the p-type contact. Finally, the DUV-LED chips were flip-chip bonded onto ceramic submounts coated with gold for light-output testing.

Characterization: The samples were characterized with optical microscopy (Olympus DX51), SEM (Hitachi S-4800; operating at 1 kV), Raman spectroscopy (Horiba, LabRAM HR-800; 514 nm laser excitation), ESEM (FEI Quanta 200F), atomic force microscopy (AFM) (BRUKER Dimension Icon), XPS (Kratos Analytical Axis-Ultra spectrometer using a monochromatic Al Kα X-ray source), TEM (FEI Tecnai F20, operating at 200 kV), and Aberration-corrected TEM (FEI Titan Cubed Themis G2 300) operated at 300 kV.

Supporting Information

Supporting Information is available from the Wiley Online Library or from the author.

Acknowledgements

Z.C. and Z.L. contributed equally to this work. The authors thank Dr. Xujing Li, Mingqiang Li, and Ning Li for help with the TEM analysis. This work was financially supported by the National Key R&D Program of China (Nos. 2018YFB0406703 and 2016YFB0400102), the National Basic Research Program of China (No. 2016YFA0200103), the National Natural Science Foundation of China (Nos. 61527814, 51432002, 61474109, 51290272, 51502007, 11474274, and 51672007), the National Equipment Program of China (ZDYZ2015-1), the Beijing Municipal Science and Technology Planning Project (Nos. Z161100002116020 and Z161100002116032), and the Beijing Natural Science Foundation (No.4182063). P.G. also appreciates the support from the National Program for Thousand Young Talents of China and the "2011 Program" Peking-Tsinghua-IOP Collaborative Innovation Center of Quantum Matter. The authors acknowledge the Electron Microscopy Laboratory at Peking University for the use of a Cs-corrected electron microscope.

Conflict of Interest

The authors declare no conflict of interest.

Keywords

aluminum nitride, chemical vapor deposition, deep-ultraviolet light-emitting diodes, graphene, quasi-van der Waals epitaxy

Received: November 13, 2018
Revised: March 23, 2019
Published online: April 16, 2019

[1] F. A. Ponce, D. P. Bour, *Nature* **1997**, *386*, 351.
[2] A. Khan, K. Balakrishnan, T. Katona, *Nat. Photonics* **2008**, *2*, 77.
[3] Y. Kobayashi, K. Kumakura, T. Akasaka, T. Makimoto, *Nature* **2012**, *484*, 223.
[4] S. Nakamura, *Science* **1998**, *281*, 956.
[5] Y. Sun, K. Zhou, Q. Sun, J. Liu, M. Feng, Z. Li, Y. Zhou, L. Zhang, D. Li, S. Zhang, M. Ikeda, S. Liu, H. Yang, *Nat. Photonics* **2016**, *10*, 595.
[6] Y. Kim, S. S. Cruz, K. Lee, B. O. Alawode, C. Choi, Y. Song, J. M. Johnson, C. Heidelberger, W. Kong, S. Choi, K. Qiao, I. Almansouri, E. A. Fitzgerald, J. Kong, A. M. Kolpak, J. Hwang, J. Kim, *Nature* **2017**, *544*, 340.
[7] J. H. Choi, A. Zoulkarneev, S. Il Kim, C. W. Baik, M. H. Yang, S. S. Park, H. Suh, U. J. Kim, H. Bin Son, J. S. Lee, M. Kim, J. M. Kim, K. Kim, *Nat. Photonics* **2011**, *5*, 763.
[8] D. G. Zhao, S. J. Xu, M. H. Xie, S. Y. Tong, H. Yang, *Appl. Phys. Lett.* **2003**, *83*, 677.
[9] H. Amano, N. Sawaki, I. Akasaki, Y. Toyoda, *Appl. Phys. Lett.* **1986**, *48*, 353.
[10] W. Kong, H. Li, K. Qiao, Y. Kim, K. Lee, Y. Nie, D. Lee, T. Osadchy, R. J. Molnar, D. K. Gaskill, R. L. Myers-Ward, K. M. Daniels, Y. Zhang, S. Sundram, Y. Yu, S.-h. Bae, S. Rajan, Y. Shao-Horn, K. Cho, A. Ougazzaden, J. C. Grossman, J. Kim, *Nat. Mater.* **2018**, *17*, 999.
[11] K. Chung, C.-H. Lee, G.-C. Yi, *Science* **2010**, *330*, 655.
[12] J. Kim, C. Bayram, H. Park, C.-W. Cheng, C. Dimitrakopoulos, J. A. Ott, K. B. Reuter, S. W. Bedell, D. K. Sadana, *Nat. Commun.* **2014**, *5*, 4836.
[13] H. Nam, C. Tran Viet, M. Han, B. D. Ryu, S. Chandramohan, J. B. Park, J. H. Kang, Y.-J. Park, K. B. Ko, H. Y. Kim, H. K. Kim,

© 2019 WILEY-VCH Verlag GmbH & Co. KGaA, Weinheim

15214095, 2019, 23, Downloaded from https://onlinelibrary.wiley.com/doi/10.1002/adma.201807345 by Zhejiang University, Wiley Online Library on [04/09/2023]. See the Terms and Conditions (https://onlinelibrary.wiley.com/terms-and-conditions) on Wiley Online Library for rules of use; OA articles are governed by the applicable Creative Commons License

J. H. Ryu, Y. S. Katharria, C.-J. Choi, C.-H. Hong, *Nat. Commun.* **2013**, *4*, 1452.
[14] S. Fernandez-Garrido, M. Ramsteiner, G. Gao, L. A. Galves, B. Sharma, P. Corfdir, G. Calabrese, Z. d. S. Schiaber, C. Pfueller, A. Trampert, J. M. J. Lopes, O. Brandt, L. Geelhaar, *Nano Lett.* **2017**, *17*, 5213.
[15] Y. Taniyasu, M. Kasu, T. Makimoto, *Nature* **2006**, *441*, 325.
[16] J. Sun, Y. Chen, M. K. Priydarshi, Z. Chen, A. Bachmatiuk, Z. Zou, Z. Chen, X. Song, Y. Gao, M. H. Ruemmeli, Y. Zhang, Z. Liu, *Nano Lett.* **2015**, *15*, 5846.
[17] L. G. Cancado, A. Jorio, E. H. Martins Ferreira, F. Stavale, C. A. Achete, R. B. Capaz, M. V. O. Moutinho, A. Lombardo, T. S. Kulmala, A. C. Ferrari, *Nano Lett.* **2011**, *11*, 3190.
[18] A. L. M. Reddy, A. Srivastava, S. R. Gowda, H. Gullapalli, M. Dubey, P. M. Ajayan, *ACS Nano* **2010**, *4*, 6337.
[19] Z. Lin, G. H. Waller, Y. Liu, M. Liu, C.-p. Wong, *Nano Energy* **2013**, *2*, 241.
[20] Y. Alaskar, S. Arafin, D. Wickramaratne, M. A. Zurbuchen, L. He, J. McKay, Q. Lin, M. S. Goorsky, R. K. Lake, K. L. Wang, *Adv. Funct. Mater.* **2014**, *24*, 6629.
[21] V. Lughi, D. R. Clarke, *Appl. Phys. Lett.* **2006**, *89*, 241911.
[22] A. H. Park, T. H. Seo, S. Chandramohan, G. H. Lee, K. H. Min, S. Lee, M. J. Kim, Y. G. Hwang, E.-K. Suh, *Nanoscale* **2015**, *7*, 15099.
[23] T. Prokofyeva, M. Seon, J. Vanbuskirk, M. Holtz, S. A. Nikishin, N. N. Faleev, H. Temkin, S. Zollner, *Phys. Rev. B* **2001**, *63*, 125313.
[24] Y. Li, Y. Zhao, T. Wei, Z. Liu, R. Duan, Y. Wang, X. Zhang, Q. Wu, J. Yan, X. Yi, G. Yuan, J. Wang, J. Li, *Jpn. J. Appl. Phys.* **2017**, *56*, 085506.
[25] V. Srikant, J. S. Speck, D. R. Clarke, *J. Appl. Phys.* **1997**, *82*, 4286.
[26] Y. Wu, A. Hanlon, J. F. Kaeding, R. Sharma, P. T. Fini, S. Nakamura, J. S. Speck, *Appl. Phys. Lett.* **2004**, *84*, 912.
[27] N. Grandjean, J. Massies, P. Vennegues, M. Laugt, M. Leroux, *Appl. Phys. Lett.* **1997**, *70*, 643.
[28] J. R. Heffelfinger, D. L. Medlin, K. F. McCarty, *J. Appl. Phys.* **1999**, *85*, 466.
[29] B. H. Le, S. Zhao, X. Liu, S. Y. Woo, G. A. Botton, Z. Mi, *Adv. Mater.* **2016**, *28*, 8446.
[30] D. Monti, M. Meneghini, C. De Santi, G. Meneghesso, E. Zanoni, J. Glaab, J. Rass, S. Einfeldt, F. Mehnke, J. Enslin, T. Wernicke, M. Kneissl, *IEEE Trans. Electron Devices* **2017**, *64*, 200.

© 2019 WILEY-VCH Verlag GmbH & Co. KGaA, Weinheim

15214095, 2019, 23, Downloaded from https://onlinelibrary.wiley.com/doi/10.1002/adma.201807345 by Zhejiang University, Wiley Online Library on [04/09/2023]. See the Terms and Conditions (https://onlinelibrary.wiley.com/terms-and-conditions) on Wiley Online Library for rules of use; OA articles are governed by the applicable Creative Commons License